Mechanics and Thermodynamics of the "Bernoulli" oscillators (uni-dimensional closed motions) Part II : Solved examples and classical limit

G. Mastrocinque

Dipartimento di Scienze Fisiche dell'Università di Napoli
"Federico II" - Facoltà di Ingegneria - P.le Tecchio - 80125 Napoli

ABSTRACT. In the previous Part I of this paper, we developed a theoretical model to account for energy and mass fluctuations in oscillators dynamics, thus providing a peculiar but classical-like insight into the quantum mechanical behaviour. The model helps with a variable density-current assumption, supported by a mass effect finding in turn its expression in what we call "the mass eigenfunctions". In the present Part II of the paper, we have worked out numerical solutions for the two basic examples of the harmonic oscillator and the (infinetely deep) rectangular well. Calculations are strongly non-linear and submitted to strict integral and differential constraints, so that we have to perform them in two steps. First the unknown function $g_n(x)$, entering the mass function expression, is taken equal to 1. This gives solutions leaving the phase quantization condition affected by a (small) error. In a second step, a numerical correction is imposed to the previous solutions in such a way that the phase errors are suppressed. So we believe having provided here detailed proof of consistency between the variable-current wave equation and the classical energy theorem (inclusive of a peculiar expression of the quantum potential inside it), whose forms we gave theoretically in the previous Part I of this work. Graphs and tables are here shown and discussed extensively for a sampled set of quantum levels of both the chosen cases. They are exhaustive, in that we can draw out from them a general insight into the classical limit. This last reveals very peculiar to our model in comparison with the JWKB standard framework.

Résumé

RÉSUMÉ. Dans un article précedent, nous avons développé un modèle théorique prenant en compte les fluctuations d'énergie et de masse dans la dynamique des oscillateurs, de façon à donner une interpretation de type classique à des effets quantiques. Le modèle s'aide avec une hypothèse de densitè de courant variable, à cause d'un effet de masse qui trouve son expression dans ce que nous appellons "les functions de masse". Dans la presente Partie II de l'article, nous avons résolu numériquement les cas de l'oscillateur harmonique et du puit de potentiel rectangulaire (infiniment profond). Les calculs sont fort non-linéaires et soumis à des fermes contraintes intégrales et différentielles, si bien qu'ils doivent se poursuivre en deux stages. Premièrement les fonctions $g_n(x)$ dans l'expression de la fonction de masse sont prises égales à 1. Cela amène à des solutions qui laissent la condition de quantisation affectée par une (petite) erreur. Dans un stage successif, on impose une correction numérique telle que l'erreur de phase est supprimée. De telle façon, nous pensons avoir demontré la congruence entre l'équation d'onde à courant variable et le théorème d'énergie classique (contenant un potentiel quantique particulier), dont les expressions sont données dans la Partie I de ce travail. Les résultats sont montrés extensivement pour un ensemble de nombres quantiques suffisant à extraire le comportement de limite classique. Ce dernier se révèle très spécial en comparaison avec le modèle standard JWKB.

PACS. 45.50.-j - Dynamics and kinematics of a particle and a system of particles

PACS. 03.65.Ta - Foundations of Quantum Mechanics

1 Introduction

In Part I of this work all the equations, with the expressions of the different variables involved and associated constraints, have been given - with the only exception of the unknown functions $g_n(\mathrm{x})$ appearing in eqs. (52 I) and (55 I). Finding the appropriate $g_n(\mathrm{x})$ values, and the numerical values of the various quoted constants (x_n, σ_n, c_n, $\rho(\mathrm{x}_n)$, ν_{n0}, τ_n, μ_n, E_{ni}, E_{nf}) able to respect the constraints, is the purpose of the calculations we are going to expound in this Part II for selected examples. The general outline of the solution procedure is as follows. For a chosen potential $\Phi(\mathrm{x})$, first we have to solve equations (4 I), (55 I) (with the Bohr postulate (23 I)) in $\rho(\mathrm{x})$ and $\nabla S(\mathrm{x})$, with the imposed conditions for these functions. The density must be a continuous function across the space, with continuous first and second derivatives ([1]); must

[1] not always true in the classical limit when a non-zero value for h is maintained, see plot (38).

be zero at the extreme boundary of the space domain and normalized to unity within it ; must reflect the potential $\Phi(\mathrm{x})$ symmetry ([2]). At the same time, continuity, symmetry and the quantization condition (8 I) must be satisfied by $\nabla S(\mathrm{x})$. All these conditions determine the values of x_n, σ_n, c_n, $\rho(\mathrm{x}_n)$, $g_n(\mathrm{x})$. For each potential, the energy values E_n are taken equal to the known values given by orthodox quantum mechanics. The values of the energies E_{ni}, E_{nf} are provided by separate analysis of the thermodynamical distributions in the dedicated sections, and ν_{n0} is consequently determined by eq.(29 I). Then $\nu_n(\mathrm{x})$, $\mathrm{v}_{_D}(\mathrm{x})$ and $\mathrm{m}_{eff}(\mathrm{x})$ can be calculated via eqs.(33 I) and (44 I) ; the constants τ_n and μ_n are determined by imposing continuity of expression (33 I) in x_n and the mass normalization equation (20 I)). At this point, all the other quantities $\mathrm{v}(\mathrm{x},\mathrm{x}_0(\mathrm{E}))$, $\mathrm{T}(\mathrm{E})$ etc. can be calculated in their turn, starting with (59 I) etc.

So our purpose now is showing indeed, and discussing with details, the solutions we have obtained for a couple of primary examples : the rectangular potential well (RW) and the harmonic oscillator (HO). The mathematical framework is strongly non-linear and we have first to deal with the problem of determining, for each n, a suitable $g_n(\mathrm{x})$. To this end, we used numerical procedures consisting of two main calculations steps. Here we start with describing them on a general basis first. Other sections in the paper will extensively display the final results for the chosen examples.

1.1 First Step Calculation : finding approximate solutions

As a first calculation step (FSC), for every chosen n we can find approximate solutions in this way. We set the function $g_n(\mathrm{x})$ to a working value 1 all over the space domain $-\mathrm{x}_n \leq \mathrm{x} \leq \mathrm{x}_n$, and calculate the values of x_n, σ_n, c_n, $\rho(\mathrm{x}_n)$ in such a way that all the imposed constraints are satisfied, with the only exception of the phase condition (8 I). Checking now on this last a posteriori, we note that it always comes out affected by a small error (not greater than $\approx$4% in the worst case (rectangular well n=2)). By numerical trials, we concluded that very accurate tuning of the function $g_n(\mathrm{x})$ around 1 is necessary to comply exactly with that condition. However, this is true only for low quantum numbers, say $\mathrm{n} \leq 5$. For greater n, indeed, the relative phase error by which solutions with $g(\mathrm{x}) = 1$ satisfy eq. (8 I) is really very small. For instance, in case n=5 for

[2] We take always x-symmetrical potentials and solutions in this paper. This implies $\rho'(0)= 0$, $\nabla S'(0) = 0$ etc.

the rectangular well, one finds the wave phase difference in a complete cycle to be 25.0669 when we have used $g(\mathrm{x}) = 1$. We have to compare it to 8π : then the RW(n=5) FSC (First Step Calculation) phase relative error is $\epsilon_p = -0.0026$. In the harmonic oscillator case, we find for HO(n=4) $\epsilon_p = -0.0054$. For HO(n=10) the FSC error is so small as $\epsilon_p = 0.0008$ and for RW(n=10) $\epsilon_p = 0.003$.

For these reasons, although the following SSC (Second Step Calculation) is applicable to all the n values below the classical limit, the FSC error for n (say) > 5 is so small that applying the correction is practically of no meaning for the demonstrative purposes of this work. Nevertheless, our calculation program being a general one in this respect, running it even for greater n was only a matter of affordable execution time (except when n start with becoming so big as ≈ 30 (RW) or ≈ 100 (HO)) so that we actually applied the correction for all the n values presented in this paper. In this way, we achieved everywhere a very good precision in fulfilling all the imposed constraints. For a full estimate of the final errors, see a comment to eq. (11) in the sequel.

1.2 Second step : refining the solutions

In order to calculate refined values of $g_n(\mathrm{x})$ and $\nabla S(\mathrm{x})$, we start with the approximate solution $\sqrt{\rho_1(\mathrm{x})}$ (index 1 here stays for $g_n(\mathrm{x}) = 1$) for the wave amplitude and we impose to it a corrective function corr(x,n) in such a way that the final solution $\rho(\mathrm{x})$ is in the form

$$\rho(\mathrm{x}) = \mathrm{corr}(\mathrm{x},\mathrm{n})^2 \rho_1(\mathrm{x}) \tag{1}$$

>From this new density, using the wave equation we can recalculate $g_n(\mathrm{x})$, $\nabla S(\mathrm{x})$ and all other consequent quantities at last. We have found that the appropriate corrective function is well fitted into a 7th degree polynome in x, since the new solution $\rho(\mathrm{x})$ must be kept firmly linked to all the continuity, symmetry and normalisation conditions quoted before ; and moreover, we ask for eq. (8 I) to be now strictly respected. Then we write in general

$$\mathrm{corr}(\mathrm{x},\mathrm{n}) = a_0 + a_1 \frac{\mathrm{x}}{\mathrm{x}_0} + a_2 \left(\frac{\mathrm{x}}{\mathrm{x}_0}\right)^2 + ...a_7 \left(\frac{\mathrm{x}}{\mathrm{x}_0}\right)^7 \tag{2}$$

For instance, in case RW(n=3), we have found by numerical analysis :

$$\mathrm{corr}(\mathrm{x},3) = 1{+}8.013410^{-4} \frac{\mathrm{x}}{\mathrm{x}_0} {+} 6.4214610^{-7} \left(\frac{\mathrm{x}}{\mathrm{x}_0}\right)^2 {+}...{+}24.4125 \left(\frac{\mathrm{x}}{\mathrm{x}_0}\right)^7 \tag{3}$$

The a_i coefficients we have used in all cases of interest can be found in Tables 2 and 4. Note that, when performing the SSC procedure, one has to recalculate the constants c_n and $\rho(\mathrm{x}_n)$. We give in tables 1 and 3, for all the constants we have used, both first and second step values.

2 Solved examples

2.1 Infinitely deep rectangular potential well (RW)

Consider the rectangular potential well [1,2] defined as

$$\Phi(\mathrm{x}) = 0 \qquad \{-\mathrm{x}_0^* < \mathrm{x} < \mathrm{x}_0^*\} \tag{4}$$

$$\Phi(-\mathrm{x}_0^*) = \Phi(\mathrm{x}_0^*) = \infty \tag{5}$$

with energy levels

$$\mathrm{E}_n = \mathrm{n}^2\mathrm{E}_1 = \frac{\mathrm{n}^2\mathrm{h}^2}{32\mathrm{m}\mathrm{x}_0^{*2}} \tag{6}$$

For each level, we locate the boundary between Region I and Region II at the abscissas

$$\mathrm{x}_n = \mathrm{x}_0^*(1 - \frac{1}{\mathrm{n}}) \tag{7}$$

For the value to be used in the classical limit, see note ([6]) in the sequel.

2.1.1 Calculation of E_{ni}, E_{nf}

The quantum thermodynamical distribution is

$$\mathrm{U}_{qm}^{RW} = \mathrm{E}_1 \frac{\sum_{n=1}^{\infty} \mathrm{n}^2 \mathrm{Exp}\left[-\frac{\mathrm{n}^2\mathrm{E}_1}{k\mathrm{T}}\right]}{\sum_{n=1}^{\infty} \mathrm{Exp}\left[-\frac{\mathrm{n}^2\mathrm{E}_1}{k\mathrm{T}}\right]} = k\mathrm{T}^2 \frac{\partial}{\partial \mathrm{T}} \mathrm{Ln}[\mathrm{EllipticTheta}[3, 0, \mathrm{Exp}(-\frac{\mathrm{E}_1}{k\mathrm{T}})]] \tag{8}$$

Turning to equation (69 I), in the RW case we have to take $c_\mathrm{v} = k/2$. Concerning U_{c0} and $\Delta\mathrm{U}$, we have found, by analytical and numerical work :

$$\mathrm{U}_{c0}(\mathrm{T}) = -0.16209 + 0.27473\ \Delta\mathrm{U}(\mathrm{T}) \tag{9}$$

$$\Delta\mathrm{U}(\mathrm{T}) = 2\mathrm{E}_1 < \mathrm{n} - \frac{1}{4} >= 2\mathrm{E}_1 \frac{\sum_{n=1}^{\infty} \left(\mathrm{n} - \frac{1}{4}\right) \mathrm{Exp}\left[-\frac{\mathrm{n}^2\mathrm{E}_1}{k\mathrm{T}}\right]}{\sum_{n=1}^{\infty} \mathrm{Exp}\left[-\frac{\mathrm{n}^2\mathrm{E}_1}{k\mathrm{T}}\right]} \tag{10}$$

With these equations indeed, it turns out that

$$\frac{< \mathrm{U} >_{fluct}^{RW}}{\mathrm{U}_{qm}^{RW}} = 1 \pm \epsilon \tag{11}$$

where $\epsilon < 0.005$ all across the temperature domain ([3]). To be simple in our theory, we did not push here our thermodynamic fit up to achieve a smaller error. Refining the model to eliminate the small discrepancy ϵ can be left indeed to future work. Then for the RW case we accepted relative errors of the order of a few thousandths, throughout all the subsequent calculations, to fulfill the model constraints. The accepted error for all the HO calculations, instead, is very much smaller ($\lesssim$0.0001).

Conclusively by the help of equations (69 I), (70 I), (10) we can take here, with very small error :

$$\mathrm{E}_{nf} = \mathrm{E}_1(\mathrm{n}^2 + \mathrm{n} - \frac{1}{4}), \quad \mathrm{E}_{ni} = \mathrm{E}_1(\mathrm{n}^2 - \mathrm{n} + \frac{1}{4}) \tag{12}$$

2.1.2 Tables and graphs from numerical solutions

Solutions for this case are traced in the following table and figures, for sampled values of n. The variable x is represented in the graphs by the normalized variable $\xi = \mathrm{x}/\mathrm{x}_0^*$. Discussion of these and other results is in a next section. FS = first step calculation, SS = second step calculation.

[3] As all our calculations, checked with an ordinary PC and software Wolfram Mathematica 8 (Lic. 4733-9644).

n	1	2	3	5
c_n(FS)	0.706981	0.94125	0.996495	1.03869
c_n(SS)	0.706981	0.911231	0.967761	1.02016
$\frac{\sigma_n}{x_0^{*2}}\|1 - c_n(SS)\|$	n.appl.	0.154484	0.712445	0.0201617
$x_0^* \rho(x_n)$ (FS)	1	0.925015	1.07787	1.33641
$x_0^* \rho(x_n)$ (SS)	1	0.950337	1.07569	1.33807
τ_n	0.25294	- 0.2689318	- 0.317113	- 0.316662
μ_n	0.31143	0.0207467	0.00008447	0.00202296

n	10	14	25	> 25 Class. Lim.
c_n(FS)	1.04054	1.02622	0.990465	1
c_n(SS)	1.0249	1.01385	0.983114	1
$\frac{\sigma_n}{x_0^{*2}}\|1 - c_n(SS)\|$	0.00870555	0.00455907	0.00644255	0
$x_0^* \rho(x_n)$ (FS)	1.89654	2.27576	3.14393	$\sqrt{\frac{n}{2}}$
$x_0^* \rho(x_n)$ (SS)	1.89277	2.2696	3.13467	$\sqrt{\frac{n}{2}}$
τ_n	-0.32355	-0.319095	-0.296064	-0.25
μ_n	0.0003166	0.00559757	0.029192	0

Table 1

n	a_0	a_1	a_2	a_3
2	1	$-9.67491\ 10^{-6}$	$9.36039\ 10^{-11}$	$6.59826\ 10^{-4}$
3	1	$8.0134\ 10^{-4}$	$6.42146\ 10^{-7}$	$1.80399\ 10^{-3}$
5	1	$-3.03166\ 10^{-6}$	$9.19096\ 10^{-12}$	$1.92497\ 10^{-3}$
10	1	$4.3535\ 10^{-6}$	$1.8953\ 10^{-11}$	$1.2662\ 10^{-2}$

n	a_4	a_5	a_6	a_7
2	- 106.751	641.139	- 1283.56	856.565
3	- 7.2468	32.5579	- 48.8187	24.4125
5	- 0.70896	2.64331	- 3.3	1.37483
10	0.568211	- 1.99003	2.24828	- 0.840007

Table 2

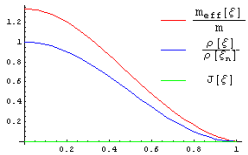

*Fig.*1) n=1

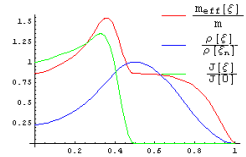

*Fig.*2) n=2

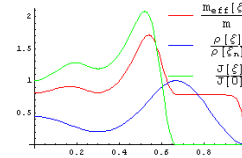

*Fig.*3) n=3

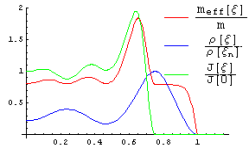

*Fig.*4) n=4

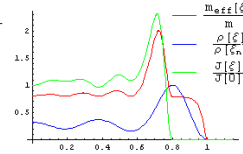

*Fig.*5) n=5

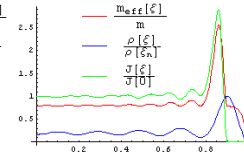

*Fig.*6) n=10

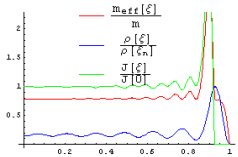

*Fig.*7) n=14

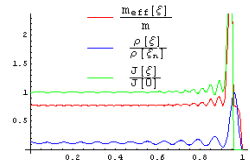

*Fig.*8) n=25

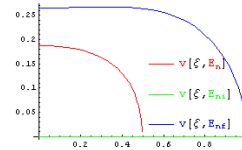

*Fig.*9) n=1

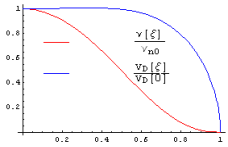

*Fig.*10) n=1

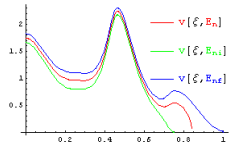

*Fig.*11) n=4

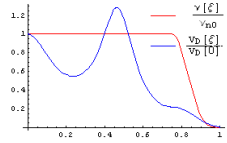

*Fig.*12) n=4

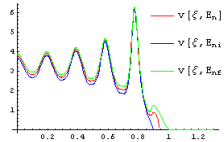

*Fig.*13) n=10

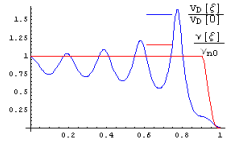

*Fig.*14) n=10

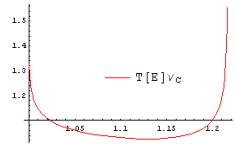

*Fig.*15) n=10

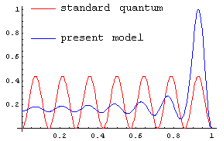

*Fig.*16) n=14

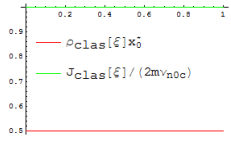

*Fig.*17) *class.*lim.

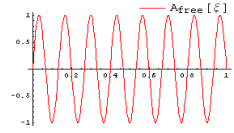

*Fig.*18) n=30

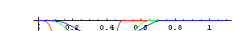

2.2 Harmonic oscillator (HO)

Consider the harmonic oscillator potential defined as

$$\Phi(\mathrm{x}) = \frac{1}{2}\,\mathrm{m}\;4\pi^2\nu_c^2\;\mathrm{x}^2 \tag{13}$$

with energies

$$\mathrm{E}_n = 2\left(\mathrm{n}-\frac{1}{2}\right)\mathrm{E}_1 = \left(\mathrm{n}-\frac{1}{2}\right)\mathrm{h}\nu_c \tag{14}$$

For each level, we locate the boundary between Region I and Region II at the abscissas x_n where the standard q.m. wavefunctions

$$\mathrm{u}_n(\mathrm{x}) \;\propto\; \mathrm{Exp}[-\frac{(2\pi\mathrm{m}\nu_c\mathrm{x})^2}{2\hbar}]\mathrm{HermiteH}[n-1,\sqrt{\frac{2\pi\mathrm{m}\nu_c}{\hbar}}\mathrm{x}] \tag{15}$$

attain their absolute maxima (for the value to be used in the classical limit, see note ([6]) in the sequel). The numerical program calculates these values : f.i. we find $\mathrm{x}_2 = \sqrt{\hbar/(2\pi\mathrm{m}\nu_c)}$.

2.2.1 Calculation of E_{ni}, E_{nf}

For the harmonic oscillator, use of equations (69 I), (70 I) is straightforward : we take $c_\mathrm{v} = k$, $\mathrm{U}_{c0} = 0$, $\Delta\mathrm{U}{=}\mathrm{h}\nu_c$ and we find

$$< \mathrm{U} >^{HO}_{fluct} = \frac{\mathrm{h}\nu_c}{\mathrm{Exp}\left[\frac{\mathrm{h}\nu_c}{k\mathrm{T}}\right]-1} + \frac{\mathrm{h}\nu_c}{2} = \mathrm{U}^{HO}_{qm} \tag{16}$$

This is indeed the qm. Bose-Einstein distribution. We obtain now easily

$$\mathrm{E}_{nf} = \mathrm{n}\;\mathrm{h}\nu_c, \qquad \mathrm{E}_{ni} = (\mathrm{n}-1)\mathrm{h}\nu_c \tag{17}$$

2.2.2 Tables and graphs from numerical solutions

Solutions for this case are traced in the following table and figures, for sampled values of n. The variable x is represented in the graphs by the normalized variable $\xi = \mathrm{x}/\mathrm{x}_2$, $\mathrm{x}_2 = \sqrt{\hbar/(2\pi\mathrm{m}\nu_c)}$. Discussion of the results is in the next section.

n	1	2	3	5
c_n(FS)	0.97538	1.15203	1.19012	1.22854
c_n(SS)	0.97538	1.13533	1.1764	1.21517
$\frac{\sigma_\mu}{x_2^2}\|1-c_n(SS)\|$	n.appl.	0.315983	0.376859	0.352285
$x_2\rho(x_n)$ (FS)	$\pi^{-\frac{1}{2}}$	0.391215	0.371453	0.356471
$x_2\rho(x_n)$ (SS)	$\pi^{-\frac{1}{2}}$	0.398818	0.372607	0.35681
τ_n	0.943211	0.0582507	0.017352	0.010
μ_n	1.08316	0.346675	0.330593	0.339613

n	10	30	80	> 100 Class. Limit.
c_n(FS)	1.24623	1.23567	1.20633	1
c_n(SS)	1.2376	1.2291	1.20026	1
$\frac{\sigma_\mu}{x_2^2}\|1-c_n(SS)\|$	0.32501	0.283446	0.247035	0
$x_2\rho(x_n)$ (FS)	0.348006	0.346689	0.351626	$\frac{\sqrt{2}}{\pi}$
$x_2\rho(x_n)$ (SS)	0.348114	0.346575	0.351626	$\frac{\sqrt{2}}{\pi}$
τ_n	0.088	0.170	0.2	-0.25
μ_n	0.446698	0.552101	0.581428	0

Table 3

n	a_0	a_1	a_2	a_3
2	1	$2.20934\ 10^{-7}$	$4.88115\ 10^{-14}$	$7.52422\ 10^{-5}$
3	1	$4.13409\ 10^{-6}$	$1.70907\ 10^{-11}$	$1.6663\ 10^{-4}$
5	1	$7.42819\ 10^{-6}$	$5.5178\ 10^{-11}$	$-4.50544\ 10^{-4}$
10	1	$-1.9991\ 10^{-7}$	$3.99691\ 10^{-14}$	$-1.63618\ 10^{-3}$
30	1	$-4.51148\ 10^{-5}$	$2.03534\ 10^{-9}$	$-1.88195\ 10^{-3}$

n	a_4	a_5	a_6	a_7
2	- 5.47273	16.4343	- 16.4506	5.48903
3	- 0.163295	0.309731	- 0.196	0.0413525
5	$-6.57693\ 10^{-3}$	$8.62937\ 10^{-3}$	$-3.636\ 10^{-3}$	$5.06148\ 10^{-4}$
10	$2.61494\ 10^{-3}$	$-1.37554\ 10^{-3}$	$3.0\ 10^{-4}$	$-2.3497\ 10^{-5}$
30	$1.37769\ 10^{-3}$	$-3.54825\ 10^{-4}$	$3.90185\ 10^{-5}$	$-1.5651\ 10^{-6}$

Table 4

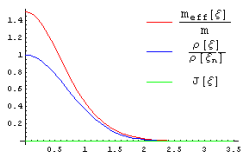

*Fig.*22) n=1

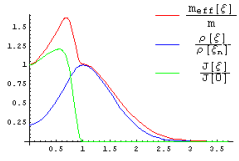

*Fig.*23) n=2

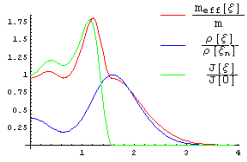

*Fig.*24) n=3

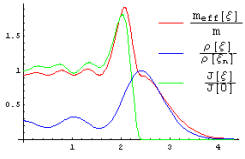

*Fig.*25) n=5

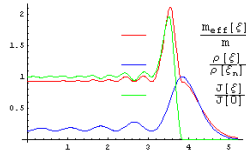

*Fig.*26) n=10

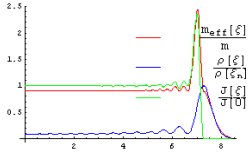

*Fig.*27) n=30

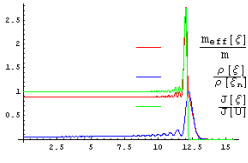

*Fig.*28) n=80

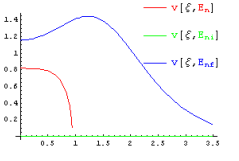

*Fig.*29) n=1

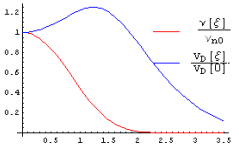

*Fig.*30) n=1

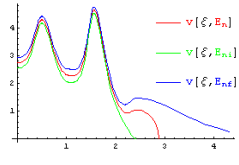

*Fig.*31) n=5

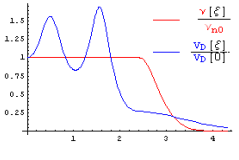

*Fig.*32) n=5

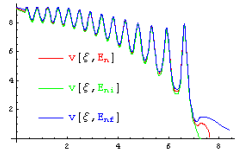

*Fig.*33) n=30

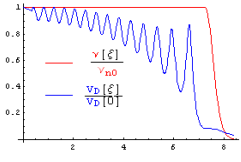

*Fig.*34) n=30

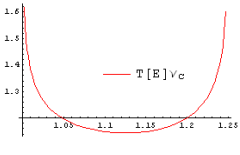

*Fig.*35) n=5

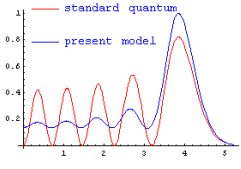

*Fig.*36) n=10

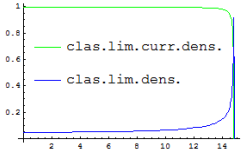

*Fig.*37) n=110

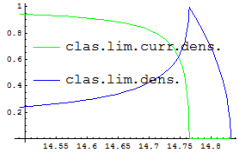

*Fig.*38) n=110

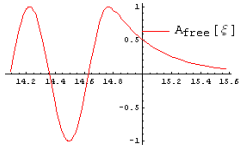

*Fig.*39) n=110

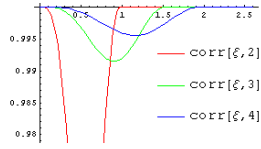

*Fig.*40) *Selected corr*[ξ,*n*] *funcs*

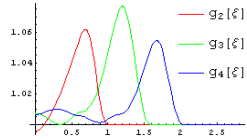

*Fig.*41) *Selected* g_n *funcs*

2.3 Discussion of the results

Our solutions ρ_n(x) (given in blue traits, plots 1÷8 for the RW and 22÷28 for the HO) look not so different from the stationary orthodox quantum mechanical densities (calculated at zero current) in their behavior ; but the modulation depth is smaller (and grows smaller with increasing n). To have an effective view, we compare directly (in plots 16 and 36, for n=14 and 10 respectively) the densities resulting from our model (blue) and the orthodox q.m. theory (red). In the RW case, it is more easily seen that the density is "attracted" towards the border where it displays an higher peak compared to the internal ones : this peak increases and narrows with increasing n. The same occurs in the HO case, although there it may be less evident because of the natural shape of the orthodox quantum mechanical density - also showing an extreme higher peak. The effective masses (in red traits, again plots 1÷8 and 22÷28) are oscillating functions as well, showing their higher peaks towards the border side and going down to 0 at the extreme boundary. Here again, the peaks increase and grow thinner with increasing n. The current densities (in green traits, same plots) are similar to the previous functions in their behaviors, but they attain a zero value just at the end of Region I and keep it firm all throughout the border region or "Region II". In this region actually, our model densities are always coincident with the orthodox q.m. ones (except for a multiplicative constant). In our plots, the Region II can be just identified as the region of space where the green traits representing a null current density run in coincidence with the horizontal axis. Other ways of looking at Region II is as the part of space lying on the right hand of the highest peaks of the density or, equivalently, as to the part of space complemental to the one where the flow functions are constants. In other diagrams, we represent for some levels the flow functions ν_n(x) and the group velocities v_D(x) (plots 10,12,14,30,32,34). As represented already in our equations, the flow functions always keep constant values in Region I, and move down

to 0 at the end of Region II. Main examples of single-particles velocity fields v(x,E), for the typical values of E = E_{ni}, E_{nf}, E_n are in plots 9,11,13,29,31,33. We do not represent other energy values but it should not to be said that the corresponding velocities are intermediate functions amongst the ones we have plotted. The velocity fields display characteristic oscillations in Region I, and after reaching a last maximum at the crossing with Region II, fall down to 0 at the appropriate turning point. There they show an infinite x-derivative as they must, because their asymptotic behavior is of the form $v(x,E) \approx \sqrt{x_{0n}(E) - x}$. Yet the group velocities $v_{_D}(x)$ may deviate from this behavior at the border, because they do not represent real single-particle velocities but the open-packets center of mass velocities. In plots (15,35) we added typical examples of periods as functions of the energy, pertaining to the velocity fields in a fluctuation interval. Abscissas in these plots are the normalized energies E/E_{ni}. The plotted periods are normalized to the corresponding classical values ν_{n0c}^{-1} calculated at the mean energy values E_n([4]). It is interesting to note that in the HO case the period function is quite a symmetrical curve around the central value E_n.

Collected examples of the corrective functions $g_n(x)$ and corr(x,n) shapes are also shown in plots (19,20,40,41) for the two cases of interest. For the RW case, where in order to calculate E_{ni} and E_{nf} a fit of the thermodynamic eq. (8) has been given in terms of (69 I), (9) and (10), the relative error ϵ affecting the ratio (11) is plotted as a function of the normalised temperature kT/E_1through a meaningful domain. As is obvious from eq.(16), the corresponding error for the HO case is right zero all over the temperature domain.

In other plots we show densities and current densities corresponding to our model "classical limit". By this expression we intend to frame the equations set when the limit $m_{eff}(x) \to m$ is attained, the constants $c_n \to 1$, and all the other appropriate assumptions (as reported in the next section) are taken. Therefore, we show f.i. (in plots 17,37,38) the quantities $\rho_{_{clas}}(x)$, and $J_{clas}(x)$ as calculated from equations (22) and (26). These so-defined quantities generally turn out not identical with the purely classical ones, if not in the very limit $h \to 0$. They are indeed given by averages of the last ones taken across the fluctuation energy interval. Our classical limit equations actually do not require setting h=0, because they always hold in the energy broadened, microcanonic-ensemble framework. Yet from the same equation we find that (only) in

[4]For the RW case, $\nu_{n0c} = 2nE_1/h$ and for the HO case $\nu_{n0c} = \nu_c$ as is obvious.

the RW case the microcanonic ensemble density is ("almost everywhere") identical with the purely classical expression $1/(2x_0^*)$ ([5]). This is a coincidence due to the potential $\Phi(x)$ being just zero (everywhere except in $x=x_0^*$) in the RW case. Then plot 17 merely reproduces the purely classical current all over the space domain except at the border point x_0^* where by eq. (26) it abruptly turns to zero. The difference between expression (22) and the purely classical density is much more evident in the HO case (see plots 37 and 38; this last is the same than 37, viewed on a different scale near the border). It must be noted that the statistical average (22) is able to cut off the classical singularity offering finite values in x_n. As is clearly shown just in plot 38, generally a discontinuous (and infinite, at left) derivative is displayed in this point. In our graphs, densities are reported normalized to their maximum value assumed in the point x_n, unless a different scale is specified; current densities are often given in arbitrary scales for the sake of a compact view of all functions in the plots. Velocity fields are in units of $h/(m\ x_0^*)$ (RW case), $\sqrt{h\nu_c/m}$) (HO case). Group velocities $v_{_D}(x)$ and flow functions $\nu_n(x)$ are simply normalized to the values they take in $x = 0$.

Finally, we solved eq. (29) for a couple of emblematic n values and plotted in Figs. 18 and 39 the pertinent functions, that we have named "vacuum free-waves" with amplitudes $A_{free}(\xi)$ as just explained in the next section. For the RW case the solution is simply a sinusoid as given in (30), because for this potential the classical limit Region II reduces to a null extension located at the extreme point $\xi_0^* = 1$. In the HO case, instead, Region II extends outside the point ξ_n up to infinity so that according to eq. (31), we have a sinusoid when $\xi < \xi_n$ (Region I) and essentially an evanescent exponential tail for $\xi \geq \xi_n$. To be simple, plot 39 only includes a small region around the border point ξ_n.

3 Classical limit

The classical limit is achieved when quantum numbers are "great enough". As it can be inferred from tables (1) and (3), this occurs when the constants c_n are very near to unity. So in our model, the quantities $|1 - c_n|$ can be interpreted as coupling constants between the vacuum and the matter. This is in agreement with the following ideas.

We want to propose here a slightly modified version of the Bohr interpretational postulate. To this end, first note the following. The quantum

[5] Everywhere, except in $x=x_0^*$ - because a purely classical density is always singular ($\to \infty$) in the turning point.

density derivatives $\rho'(\mathrm{x})$ and $\rho''(\mathrm{x})$ must be continuous functions everywhere in the space so we have to solve our equations with the condition $\rho'(\mathrm{x}_n)= 0$. But in the classical limit, $\mathrm{m}_{eff}(\mathrm{x})\rightarrow\mathrm{m}$, so that - by the structure of equation (22 I) (which becomes, in the present context, (22)) - $\rho'(\mathrm{x})$ is discontinuous in x_n. It is finite and generally $\neq 0$ in x_n^+ (i.e. $\mathrm{x}\rightarrow\mathrm{x}_n$ from "right", staying in Region II) ; while it attains an infinite value in x_n^- ($\mathrm{x}\rightarrow\mathrm{x}_n$ from "left", staying in Region I). We name therefore $\rho'(\mathrm{x}_n^{\pm})$ the $\rho'(\mathrm{x})$ limits for $\mathrm{x}\rightarrow\mathrm{x}_n^{\pm}$, and write now by definition :

$$A(\mathrm{x}) = \pm\,|1-\mathrm{c}_n|\,\sqrt{\rho(\mathrm{x})} \pm \mathrm{x}_n^2\rho'(\mathrm{x}_n^+)A_{free}(\mathrm{x}) \tag{18}$$

Here we assign to the new function $A_{free}(\mathrm{x})$ the role of a vacuum wave amplitude "not linked" ($= free$) to the matter wavefunction amplitude $\sqrt{\rho(\mathrm{x})}$. Yet this "free" wave is always generated by the particle moving in the vacuum. Consider now equation (57 I) : when we want to work out quantum-like solutions, we choose $\rho'(\mathrm{x}_n^{\pm})= 0$ and eq. (18) practically goes back to the Bohr postulate (here a constant apart). When we turn to the classical limit, we take instead $\mathrm{c}_n = 1$, $\rho'(\mathrm{x}_n^+)\neq 0$, and we write

$$\mathrm{m}_{eff}(\mathrm{x}) = \mathrm{m}_{eff}(\mathrm{x}_n) = \mathrm{m} \qquad \{\text{Region I}\} \tag{19}$$

$$\mathrm{m}_{eff}(\mathrm{x}) = \mathrm{m} = \frac{\mathrm{h}\;\nu_n(\mathrm{x})}{2\,\mathrm{v}_{_D}(\mathrm{x})^2} \qquad \{\text{Region II}\} \tag{20}$$

This last implies in eq. (32 I) :

$$\mu_n \;= 0, \quad \tau_n \;= -1/4 \tag{21}$$

Eq. (22 I) now becomes

$$< \rho_{_{clas}}(\mathrm{x},\mathrm{x}_{0n}(\mathrm{E})) >_{(n>>1)} \;= \frac{2\sqrt{2\mathrm{m}}}{\mathrm{h}}\left(\sqrt{\mathrm{E}_{nf}-\Phi(\mathrm{x})} - \mathrm{Re}\,\sqrt{\mathrm{E}_{ni}-\Phi(\mathrm{x})}\right) \tag{22}$$

and eq. (59 I) writes

$$\frac{1}{2}\,\mathrm{m}\;\mathrm{v}(\mathrm{x},\mathrm{x}_{0n}(\mathrm{E}))^2+\Phi(\mathrm{x}) + \frac{\mathrm{h}\nu_{n0}}{2} - \mathrm{h}\nu_n(\mathrm{x}) - \frac{\hbar^2}{2\mathrm{m}}\,\frac{A_{free}(\mathrm{x})''}{A_{free}(\mathrm{x})} = \mathrm{E} \tag{23}$$

with solution

$$\frac{1}{2}\,\mathrm{m}\;\mathrm{v}(\mathrm{x})^2+\Phi(\mathrm{x}) \;= \mathrm{E} \tag{24}$$

$$-\frac{\hbar^2}{2\mathrm{m}}\,\frac{A_{free}(\mathrm{x})''}{A_{free}(\mathrm{x})} = -\frac{\mathrm{h}\nu_{n0}}{2} + \mathrm{h}\nu_n(\mathrm{x}) \tag{25}$$

So adding eq. (4 I) we have now ([6])

$$\frac{\nabla S_{class}(\mathrm{x})^2}{2\mathrm{m}} = [\mathrm{E}_{ni} - \Phi(\mathrm{x})]\,\mathrm{UnitStep}[\mathrm{x}_n - \mathrm{x}] \tag{26}$$

and

$$\Psi_{class}(\mathrm{x}) = \Psi_{free}(\mathrm{x}) = A_{free}(\mathrm{x})\exp(iS_{class}(\mathrm{x})/\hbar) \tag{27}$$

>From these equations, it is clear that in our model attaining the classical limit does not require setting h→ 0 in any of the equations at all. The Planck constant is a real physical constant always playing its role even in the classical world, where it simply generates a vacuum motion (without feedback on matter) with a classical-limit wavefunction $\Psi_{class}(\mathrm{x})$. Feedback only arises when we set $\rho'(\mathrm{x}_n)= 0$ (at the same time we have $\mathrm{c}_n \neq 1$), what insures coupling with the particle density in the quantum world. The classical energy theorem (24) is recovered integrally, but let us point out again the interpretational context : for the sake of rigour in the model, the energy E must not be regarded, here again, as a single-valued constant for each particle, but always participates of an interval of possible values between E_{ni}, E_{nf} in the microcanonic ensemble. Referring now the form (24) to only one real particle, the final interpretation we give to this equation is that even in the classical world ergodicity must be invoked : so a very slow (and weak, $\mathrm{E}_{nf} - \mathrm{E}_{ni} << \mathrm{E}$) time-fluctuation E(t) due to the vacuum influence always affects the classical motions, in agreement with the postulate (63 I) and the overall fluctuation framework we have installed. Postulate (63 I) should be written now using the classical periods for the energy densities, and values of τ great enough so that no appreciable frequency of the fluctuation (a quantum-like effect) is actually measurable during the ordinary observation times of a classical motion.

Since in the classical ensemble ($\mathrm{m}_{eff}(\mathrm{x})$=m) $\rho'(\mathrm{x}_n^-)\rightarrow \infty$, it is perhaps preferable re-defining eq. (18) in the form

$$A(\mathrm{x}) = \pm\sqrt{\rho(\mathrm{x})} \pm \mathrm{x}_n^2\rho'(\mathrm{x}_n^-)A_{free}(\mathrm{x}) \tag{28}$$

[6] In eqs. (25), (26) the classical limit values of x_n, to be taken in the RW and HO cases, are equal to x_0^* and $\sqrt{\frac{(\mathrm{n}-1)\hbar}{\pi \mathrm{m}\nu c}}$ respectively.

In this way the quantum solutions with $\rho'(\mathrm{x}_n^-)= 0$ agree exactly with the known expression of the Bohr postulate. Then the contribution of $A_{free}(\mathrm{x})$ moves to a function with negligeable amplitude in the quantum world ([7]).

It is now easy to introduce a refinement to eq. (25) : it is de-coupled from the energy theorem, so we are allowed to take it apart now from the global context, and write it again inserting a constant χ_n^2 more into it :

$$-\chi_n^2 \frac{\hbar^2}{2\mathrm{m}} \frac{A_{free}(\mathrm{x})''}{A_{free}(\mathrm{x})} = -\frac{\mathrm{h}\nu_{n0}}{2} + \mathrm{h}\nu_n(\mathrm{x}) \tag{29}$$

This is tantamount to say that unity is replaced by a value χ_n^2 in the classical limit. In this way we can write the solutions for $A_{free}(\xi)$ (ξ is the normalized space variable as previously defined for RW and HO) in the good form to preserve the right number of nodes :

$$A_{free}(\xi) \mid_{n>>1} = A_{free}(\xi_n)\mathrm{Sin}[\mathrm{n}\frac{\pi}{2}(1-\xi)] \qquad \{\text{RW case, } \xi_n = 1\} \tag{30}$$

$$A_{free}(\xi) \mid_{n>>1} = A^{\mathrm{I}}_{free}(\xi_n)\mathrm{Cos}[(\mathrm{n}-1)\frac{\pi}{2}\left(1-\frac{\xi}{\xi_n}\right)]\,\mathrm{UnitStep}[\xi_n - \xi] +$$

$$+A^{\mathrm{II}}_{free}(\xi)\,(1-\mathrm{UnitStep}[\xi_n-\xi]\,) \quad \left\{\text{HO case, } \xi_n = \sqrt{2\mathrm{n}-2}\right\} \tag{31}$$

The last are obviously submitted to continuity in ξ_n, and to the choice of a norm condition giving $A^{\mathrm{I}}_{free}(\xi_n)$. On the other hand, from eq. (29) easily follows that (for potentials different from RW-like) $A^{\mathrm{II}}_{free}(\xi)$ includes an evanescent tail in the space where $\nu_n(\mathrm{x}) < \nu_{n0}/2$. This has indeed been shown in plot 39 for the HO case. To insure solutions (30) and (31) we have to take :

$$\chi_n^2 = \frac{1}{\mathrm{n}} \qquad \left\{\rho'(\mathrm{x}_n^+) \neq 0,\ \text{RW case, class. limit}\right\} \tag{32}$$

$$\chi_n^2 = \frac{8}{\pi^2\,(\mathrm{n}-1)} \quad \left\{\rho'(\mathrm{x}_n^+) \neq 0,\ \text{HO case, class. limit}\right\} \tag{33}$$

When $\mathrm{n}\to\infty$, $\chi_n^2 \to 0$ in both cases. Looking now again at the quantum-like solutions, from calculations shown in Tables 1) and 3) - together with

[7] When $\rho'(\mathrm{x}_n^-)\to\infty$ instead, the amplitude $A(\mathrm{x})\to\infty$ as well but the real physics here rests on the Bohm potential value$\propto A(\mathrm{x})''/A(\mathrm{x})$ which obviously stands up finite.

a few other projections that can be made - we evaluate that the coefficients c_n turn to the unity when the quantum numbers attain say one or two hundreds (just to fix ideas). We note that in the HO case the progression of the coefficients τ_n and μ_n towards the classical limit values ($-1/4$ and 0 respectively) looks not traced yet in the table, since sufficiently high values of n are not attained there. In our model however, when the energy E_n gets smaller than a critical (so, rather high) value, the coefficients $1-c_n$ start with becoming different from zero ; this is the reason why we have interpreted them as coupling constants with the vacuum. This step marks the transition from the classical state to a quantum mechanical state : i.e. to a strong coupling of the vacuum wave with the material density, where the vacuum wave amplitude is able to drive the latter in agreement with the Bohr postulate.

Then at the critical and smaller energies, the coefficients χ_n^2 switch on to a value

$$\chi_n^2 = 1 \qquad \left\{ \rho'(x_n^+) = 0, \text{ both cases, q.m.-like solutions} \right\} \tag{34}$$

jumping from values (32) or (33) to unity.

The theoretical variation due to appearance of χ_n is easily embodied into the quantization formalism. We can simply reset the momentum operator $\hat{p}$, the imaginary potential and the wavefunction definitions in (39 I), (40 I), (7 I) as follows :

$$\hat{p} = i\chi_n \frac{h\nabla_x}{2\pi} \tag{35}$$

$$\Phi_{im}(x) = \chi_n \frac{h\, v_{_D}(x)}{4m\,\pi} \frac{d}{dx} \left(m_{eff}(x) - \frac{c_n h \nu_n(x)}{2 v_{_D}(x)^2} \right) \tag{36}$$

$$\Psi_n(x,\chi_n) = A(x) \exp\left[iS(x)/(\chi_n \hbar) \right] \tag{37}$$

Analogous corrections must be applied in the corresponding equations of the classical-part of the model, as f.i. eq.(23).

Whether our free quantum waves are observable physical elements or not, is obviously an exorbitant topic from this work. But a suggestive idea to be investigated in this respect seems to us being the possible connection to distant effects nowadays well known to play a physical role in the quantum world.

4 Conclusion

In this paper, we have shown that using an Hamiltonian (39 I) with the imaginary potential (40 I) brings the quantum-mechanical hydrodynamic equations to be solved consistently with a classical-like theorem of the form (59 I), provided we add to this frame a fluctuating energy statistics with implied flow functions $\nu_n(\mathrm{x})$, and the ergodic assumption (63 I). In eq. (59 I), as well as in the imaginary potential definition, a characteristic mass function $\mathrm{m}_{eff}(\mathrm{x})$ takes a dominant role. It appears as a new physical actor able to reconciliate (at the basic level here presented at least) the quantum theory with the classical. We have given detailed expressions of the mass functions as well as of the other quantities involved by the model, and showed in sampled graphs the solutions we obtained numerically for the two most important cases of the rectangular well and harmonic oscillator. Consistence of the global model with main thermodynamic quantum properties has also been shown, and used for the practical purpose of finding the appropriate extreme energy values of the fluctuation intervals for the cases at hand. The classical limit framework associated to the model has also been investigated. As recalled in Part I, numerical calculations of the tunnel effect as reviewed in the light of this model can also be performed and we have recently given numerical results of this approach in [4]. We believe a meaningful three dimensional motion model can also be set up in the same spirit by adding angular momentum fluctuations [5,6] and linear motions superposition techniques.

References

[1] LANDAU L. D. and LIFSCHITZ E. M., Mécanique (§ 30), Mir, Moscou (1969)
[2] MESSIAH A., Quantum Mechanics vol.I, North Holland Publ. Comp., Amsterdam (1969)
[3] MAVROMATIS H. A., Exercises in Quantum Mechanics, D. Reidel Publ. Comp., Dordrecht (1987)
[4] MASTROCINQUE G., Comm. to XCVI Congr.SIF Sez. VI, Bari, 20-24 Sept. (2010)
[5] OUDET X., Ann. de la Fond. L. de Broglie, 25, 1 (2000)
[6] OUDET X., Comm. to XCVII Congr.SIF Sez. VI, L'Aquila, 26-30 Sept. (2011)

(Manuscrit reçu le 30 juin 2011)